Published OnlineFirst June 30, 2009; DOI: 10.1158/0008-5472.CAN-09-0700
Published Online First on June 30, 2009 as 10.1158/0008-5472.CAN-09-0700

Compartment-Specific Roles of ATP-Binding Cassette Transporters Define Differential Topotecan Distribution in Brain Parenchyma and Cerebrospinal Fluid

Jun Shen,[1,2] Angel M. Carcaboso,[1] K. Elaine Hubbard,[1] Michael Tagen,[1] Henry G. Wynn,[1] John C. Panetta,[1] Christopher M. Waters,[2] Mohamed A. Elmeliegy,[1,2] and Clinton F. Stewart[1,2]

[1]Department of Pharmaceutical Sciences, St. Jude Children's Research Hospital and [2]University of Tennessee Health Science Center, University of Tennessee, Memphis, Tennessee

Abstract

Topotecan is a substrate of the ATP-binding cassette transporters P-glycoprotein (P-gp/MDR1) and breast cancer resistance protein (BCRP). To define the role of these transporters in topotecan penetration into the ventricular cerebrospinal fluid (vCSF) and brain parenchymal extracellular fluid (ECF) compartments, we performed intracerebral microdialysis on transporter-deficient mice after an intravenous dose of topotecan (4 mg/kg). vCSF penetration of unbound topotecan lactone was measured as the ratio of vCSF-to-plasma area under the concentration-time curves. The mean ± SD ratios for wild-type, *Mdr1a/b*$^{-/-}$, *Bcrp1*$^{-/-}$, and *Mdr1a/b*$^{-/-}$*Bcrp1*$^{-/-}$ mice were 3.07 ± 0.09, 2.57 ± 0.17, 1.63 ± 0.12, and 0.86 ± 0.05, respectively. In contrast, the ECF-to-plasma ratios for wild-type, *Bcrp1*$^{-/-}$, and *Mdr1a/b*$^{-/-}$*Bcrp1*$^{-/-}$ mice were 0.36 ± 0.06, 0.42 ± 0.06, and 0.88 ± 0.07. Topotecan lactone was below detectable limits in the ECF of *Mdr1a/b*$^{-/-}$ *mice*. When gefitinib (200 mg/kg) was preadministered to inhibit Bcrp1 and P-gp, the vCSF-to-plasma ratio decreased to 1.29 ± 0.09 in wild-type mice and increased to 1.13 ± 0.13 in *Mdr1a/b*$^{-/-}$*Bcrp1*$^{-/-}$ mice, whereas the ECF-to-plasma ratio increased to 0.74 ± 0.14 in wild-type and 1.07 ± 0.03 in *Mdr1a/b*$^{-/-}$*Bcrp1*$^{-/-}$ mice. Preferential active transport of topotecan lactone over topotecan carboxylate was shown *in vivo* by vCSF lactone-to-carboxylate area under the curve ratios for wild-type, *Mdr1a/b*$^{-/-}$, *Bcrp1*$^{-/-}$, and *Mdr1a/b*$^{-/-}$*Bcrp1*$^{-/-}$ mice of 5.69 ± 0.83, 3.85 ± 0.64, 3.61 ± 0.46, and 0.78 ± 0.19, respectively. Our results suggest that Bcrp1 and P-gp transport topotecan into vCSF and out of brain parenchyma through the blood-brain barrier. These findings may help to improve pharmacologic strategies to treat brain tumors. [Cancer Res 2009;69(14):5885–92]

Introduction

Malignant central nervous system (CNS) tumors carry a poor prognosis and are the most common solid tumors in children (1). Surgical resection and radiotherapy have been the cornerstones of treatment for most brain tumors, but chemotherapy is gaining an equally important role. In children ages <3 years, chemotherapy is preferentially given to avoid or delay irradiation of the developing brain (2). Because drugs approved for adults, such as temozolomide, have not shown efficacy in pediatric trials (3), new agents are needed to treat childhood brain tumors.

Camptothecin analogues (topotecan and irinotecan) exerted potent antitumor activity in xenograft models of human primary CNS tumors, including glioma, medulloblastoma, and ependymoma (4–6). Subsequent research in nonhuman primates showed that topotecan readily penetrates into the cerebrospinal fluid (CSF; ref. 7), and clinical trials showed the activity of topotecan against pediatric CNS tumors that are disseminated through the subarachnoidal space (8). However, topotecan given as a single agent has shown no activity against high-grade gliomas in children (9, 10). These disparate results may be explained in part by different drug penetration of the blood-brain barrier (BBB) and the blood-CSF barrier (BCB; ref. 11).

Among the functional components of the BBB and the BCB (for reviews, see refs. 12–14), proteins of the ATP-binding cassette (ABC) transporter family appear to play a significant role in transporting topotecan (15, 16) and are likely to affect its distribution in the brain parenchyma and CSF compartments (17–19). The ABC transporters are expressed in the brain vascular endothelial cells in the BBB and in the monolayer of ependymal cells of the choroid plexus in the BCB (20). They can also be present on the surface of tumor cells, and several *in vitro* studies have shown that tumors overexpressing the ABC transporters human breast cancer resistance protein (BCRP/ABCG2), P-glycoprotein (P-gp/MDR1/ABCB1), or multidrug resistance protein 4 (MRP4/ABCC4) are resistant to topotecan (21–23).

Transgenic rodent models in which specific transporters are deleted provide a powerful tool for examining the roles of individual transporters in the brain distribution of drugs. Our previous studies in a Mrp4-deficient mouse model suggested that Mrp4 reduces topotecan penetration into the ventricular CSF (vCSF; ref. 18). However, we observed very high vCSF accumulation of topotecan in wild-type mice (17), strongly suggesting that other drug transporters actively move topotecan from the brain parenchyma or blood into the vCSF. As topotecan is also a substrate of Bcrp1 and P-gp (16, 23, 24), these two transporters are likely to be responsible for the robust movement of topotecan across the BCB. Using immunohistochemistry, we observed the expression of Bcrp1 on the apical side of the ependymal cells of the choroid plexus and the uniform presence of P-gp in the ependymal cell cytoplasm. We also confirmed that gefitinib, a tyrosine kinase inhibitor, impedes topotecan transport into the CSF probably by inhibiting the ABC transporters at the BCB (17).

In the present study, we examined the individual roles of Bcrp1 and P-gp at the BBB and BCB by using knockout mouse models

Note: Supplementary data for this article are available at Cancer Research Online (http://cancerres.aacrjournals.org/).

Requests for reprints: Clinton F. Stewart, Department of Pharmaceutical Sciences, St. Jude Children's Research Hospital, 262 Danny Thomas Place, Memphis, TN 38105-2794. Phone: 901-595-3665; Fax: 901-525-6869; E-mail: clinton.stewart@stjude.org.

doi:10.1158/0008-5472.CAN-09-0700

Published OnlineFirst June 30, 2009; DOI: 10.1158/0008-5472.CAN-09-0700

lacking Bcrp1, P-gp, or both proteins, gefitinib as a potent inhibitor of the ABC transporters, and an intracerebral microdialysis sampling technique. We found that the presence of these proteins at the BBB and BCB explains the transport of topotecan into the vCSF and the efflux of topotecan from the brain parenchyma. These findings improve our understanding of active mechanisms regulating drug penetration into the CNS and enhance our ability to develop more effective brain tumor chemotherapy.

Materials and Methods

Drugs and chemicals. Topotecan hydrochloride (Hycamtin; GlaxoSmithKline) was prepared in sterile water (1 mg/mL). Gefitinib tablets (Iressa; AstraZeneca; 250 mg) were pulverized, and the powder was reconstituted with 0.5% Tween 20 (20%, v/v) and suspended in carboxymethylcellulose (0.25%, w/v) to a final concentration of 40 mg/mL. All other solvents and chemicals used were analytical grade or better.

Animals. FVB wild-type, *Bcrp1*$^{-/-}$, *Mdr1a/b*$^{-/-}$, and *Mdr1a/b*$^{-/-}$*Bcrp1*$^{-/-}$ female mice weighing 20 to 25 g were purchased from Taconic. All gene knockouts were created on the FVB genetic background. All procedures were approved by the St. Jude Institutional Animal Care and Use Committee and met the guidelines of the Association for Assessment and Accreditation of Laboratory Animal Care.

Topotecan plasma protein binding. Topotecan lactone plasma protein binding was determined as reported previously (17). The unbound fraction was calculated as the proportion of unbound plasma topotecan lactone to total plasma topotecan lactone.

Cannula implantation for microdialysis. The implantation of a guide cannula in anesthetized mice for microdialysis study of vCSF (25) or extracellular fluid (ECF; refs. 17, 26) has been reported. Briefly, for vCSF microdialysis, a MD-2255 guide cannula (Bioanalytical Systems) was inserted into the lateral ventricle at an angle of 20° posterior (1 mm lateral, 0.8 mm posterior, and 2 mm ventral to the bregma point). For ECF microdialysis, the guide cannula was inserted vertically into the striatum (1.8 mm lateral, 0.6 mm anterior, and 2 mm ventral to the bregma point). Mice were then allowed 3 to 5 days to recover.

Microdialysis studies. The microdialysis procedure and probe calibration have been described in detail (17, 26). Briefly, on the day of an experiment, the microdialysis probe (MD-2211; Bioanalytical Systems) was primed and flushed with artificial CSF (27). The probe was inserted through the cannula into the brain lateral ventricle or striatum, and the artificial CSF perfusion rate was set at 0.5 μL/min. The probe was allowed to equilibrate *in vivo* for at least 1 h. Topotecan (4 mg/kg) was then administered by intravenous bolus via the lateral tail vein. Gefitinib-pretreated animals received a 200 mg/kg gefitinib dose by oral gavage 1 h before topotecan. After the injection of topotecan, the dialysate samples were directly loaded onto a sample loop (2 μL) and topotecan lactone and carboxylate were simultaneously analyzed through an online microbore high-performance liquid chromatography system until topotecan concentration was undetectable (26). Topotecan carboxylate and lactone concentrations in ECF or vCSF were first corrected for the hydrolysis of topotecan lactone in pH 7.4 artificial CSF using previously described method (26). Probe recovery was determined by the *in vivo* retrodialysis method after each experiment (26). After the microdialysis experiment, the mice were euthanized and their brains were fixed in 10% neutral buffered formalin for 24 h and embedded in paraffin. H&E-stained sections (4 μm) were examined microscopically to confirm the location of the microdialysis probe track. Three to six animals were used for each condition studied.

Topotecan plasma pharmacokinetics. As in our previous murine microdialysis studies (17), we assessed plasma population pharmacokinetics in a preliminary group of mice. These results were then used as a prior distribution when assessing individual mouse plasma pharmacokinetics with limited sampling in the microdialysis studies. We estimated the plasma population pharmacokinetic parameters in each genotype and treatment group (topotecan 4 mg/kg intravenously alone versus after pretreatment with oral gefitinib 200 mg/kg) as described previously (17). Briefly, each preliminary study included six to seven mice, and blood was sampled from each mouse randomly at four of five time points (0.25, 0.5, 1.5, 3, and 6 h after drug administration chosen based on our previous experience with topotecan murine pharmacokinetic studies) either by retro-orbital bleed or (at the final time point) by cardiac puncture. Sample processing and topotecan lactone and carboxylate bioanalysis have been reported in detail. A two-compartment model was used to describe the topotecan lactone data and a third compartment was included to account for the topotecan carboxylate, and the population parameters were estimated by nonlinear mixed-effects modeling (NONMEM version VI; refs. 28, 29).

For each microdialysis experiment, three plasma samples were collected from the retro-orbital plexus (0.25, 1, and 3 h after topotecan administration; ref. 17) for plasma pharmacokinetic analysis. The above-described plasma pharmacokinetic model for topotecan was fit to the plasma topotecan lactone and carboxylate concentration-time data using maximum *a posteriori* probability Bayesian estimation (with the prior parameter distribution determined above) as implemented in ADAPT II (30). The plasma area under the curve (AUC) from zero time to infinity ($AUC_{0\rightarrow\infty}$) for unbound topotecan lactone and carboxylate was calculated by integration of the simulated concentration-time data from the model estimates. These simulated plasma AUCs were used to calculate the plasma lactone-to-carboxylate ratio of unbound topotecan.

Three-compartment analysis of combined plasma and brain topotecan lactone pharmacokinetic data. A three-compartment pharmacokinetic model (two compartments to describe the plasma topotecan lactone and one for the microdialysis obtained brain unbound topotecan lactone concentrations) was fit to the vCSF or ECF data. Specifically, topotecan lactone plasma pharmacokinetic parameters including volume of central compartment (V_c), systemic clearance (CL_t), volume of peripheral compartment (V_p), and intercompartmental clearance (CL_p) for each mouse were fixed at the values obtained by the methods described in the above section. Then, the model parameters describing the brain disposition (CL_{in}, CL_{out}, and V_{ECF} or V_{CSF}) were estimated by maximum likelihood estimation via ADAPT II (17, 31). The vCSF or ECF $AUC_{0\rightarrow\infty}$ for unbound topotecan lactone was calculated by integration of the simulated concentration-time data from the model estimates.

CNS penetration estimation. The CNS penetration of topotecan lactone was measured as the ratio of the unbound topotecan lactone AUC in brain ECF ($AUC_{u,ECF}$) or vCSF ($AUC_{u,vCSF}$) to that in plasma ($AUC_{u,plasma}$; ref. 31). The CL_{in}-to-CL_{out} ratio is also considered to express the extent of CNS penetration of topotecan lactone in the three-compartment analysis (32). Thus, we compared the topotecan penetration estimates calculated by both approaches based on the relationship $AUC_{brain}/AUC_{plasma} = CL_{in}/CL_{out}$ (32).

Immunohistochemistry. The brains of FVB wild-type, *Bcrp1*$^{-/-}$, and *Mdr1a/b*$^{-/-}$ mice were fixed overnight in 10% neutral buffered formalin and embedded in paraffin. The presence of Bcrp1 was immunohistochemically assessed in the sectioned tissues as reported previously (17). The area and intensity of staining in digital images was quantified using NIH ImageJ software. After background subtraction, the stained area was assessed by setting the threshold of the red channel of each image at 4 SDs below the mean pixel intensity and calculating the integrated intensity of the selected area. Bcrp1 staining area and intensity values were normalized to the mean values of negative control slides.

***In vitro* study of topotecan lactone and carboxylate transport by BCRP.** To assess BCRP transport of topotecan lactone and carboxylate, BCRP-expressing Saos2 cells (Saos-BCRP; ref. 23) and Saos2-pcDNA control cells were incubated with topotecan at different pH values to shift the distribution of the lactone (pH 6) and carboxylate (pH 8) forms. Cells (1×10^6) were incubated in DMEM (10% fetal bovine serum, 1% L-glutamine) in 10 cm^2 dishes for 16 h at 37°C. The medium was carefully aspirated and the cells were washed twice with PBS (pH 6 or 8). For topotecan treatment at pH 6, a topotecan stock solution in DMSO was diluted to 500 ng/mL in pH 6 PBS (37°C). For topotecan treatment at pH 8, a topotecan stock solution in 0.4 N borax solution was diluted to 500 ng/mL in pH 8 PBS (37°C). The prepared topotecan treatment solutions (8 mL) were added to each 10 cm^2 dish (n = 3). After incubation for 1 or 30 min at 37°C without CO_2, the

Published OnlineFirst June 30, 2009; DOI: 10.1158/0008-5472.CAN-09-0700

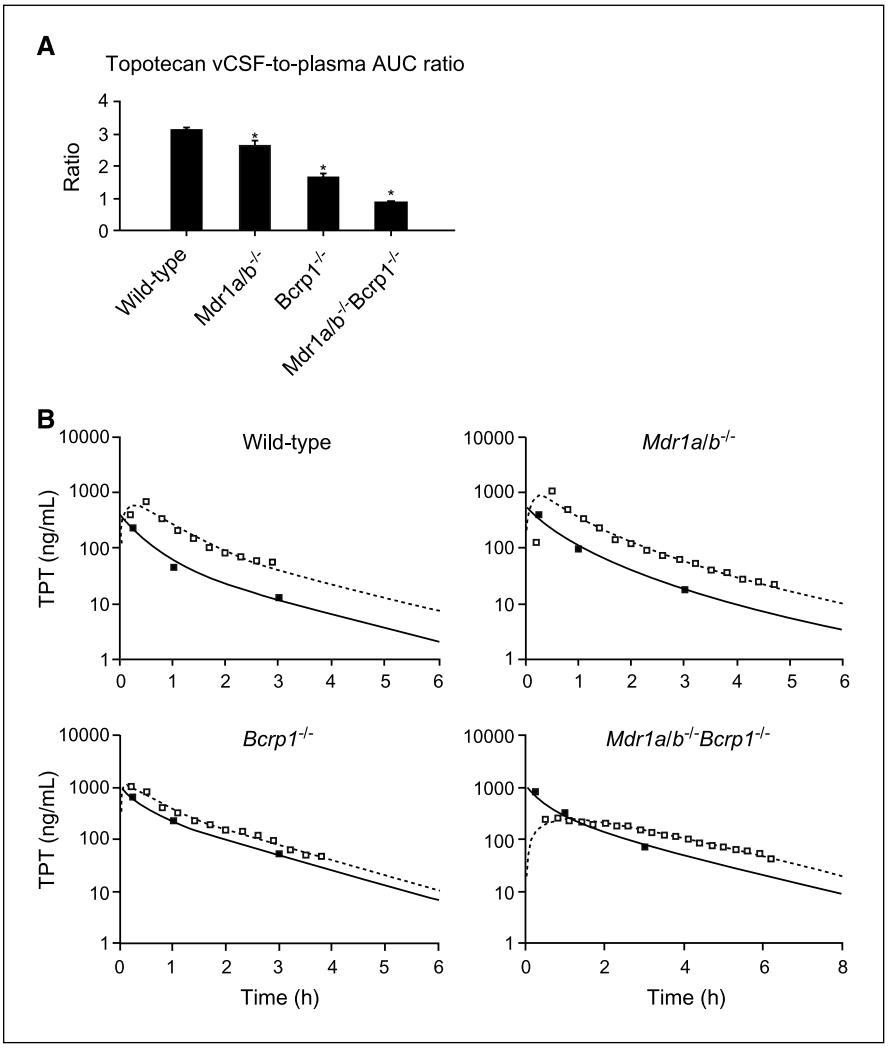

Figure 1. Topotecan lactone penetration of vCSF after a bolus intravenous dose of 4 mg/kg topotecan. *A,* vCSF-to-plasma AUC ratio of unbound topotecan lactone (mean ± SD from 3 to 6 mice). $P < 0.001$, one-way ANOVA; *, $P < 0.001$, post hoc *t* test with Bonferroni correction, of each knockout model compared with wild-type mice. *B,* representative concentration-time plots of unbound topotecan lactone (*TPT*) in vCSF (□) and plasma (■) in wild-type, *Mdr1a/b*$^{-/-}$, *Bcrp1*$^{-/-}$, and *Mdr1a/b*$^{-/-}$*Bcrp1*$^{-/-}$ mice. Model-fitted curves are represented for plasma and brain pharmacokinetic data.

treatment medium was removed, the plate was washed once with 5 mL cold PBS at pH 6 or 8, respectively, 1 mL PBS at pH 6 or 8 was added to the dishes, and the cells were detached by using a cell scraper. The cells were then ultrasonically lysed (10 s × 3). The lysate (200 μL) was added to 800 μL cold methanol for topotecan extraction to determine the intracellular drug concentration. Proteins in the remaining lysate were quantified by colorimetric assay (Dc Protein Assay; Bio-Rad Laboratories).

Statistics. In cases where two groups were compared, a Student's *t* test was done. For the comparison of more than two groups, a one-way ANOVA was done followed by a post hoc *t* test with Bonferroni correction.

Table 1. Unbound topotecan lactone vCSF-to-plasma and ECF-to-plasma AUC ratios and CL_{in}-to-CL_{out} ratios

Group	vCSF		ECF	
	AUC ratio	CL_{in}-to-CL_{out}	AUC ratio	CL_{in}-to-CL_{out}
Topotecan 4 mg/kg				
FVB wild-type	3.07 ± 0.09	3.01 ± 0.15	0.36 ± 0.06	0.36 ± 0.06
Mdr1a/b$^{-/-}$	2.57 ± 0.17	2.57 ± 0.17	N/A	N/A
Bcrp1$^{-/-}$	1.63 ± 0.12	1.59 ± 0.16	0.42 ± 0.06	0.42 ± 0.06
Mdr1a/b$^{-/-}$*Bcrp1*$^{-/-}$	0.86 ± 0.05	0.86 ± 0.04	0.88 ± 0.07	0.89 ± 0.07
Topotecan 4 mg/kg + gefitinib 200 mg/kg				
FVB wild-type	1.29 ± 0.09	1.25 ± 0.14	0.74 ± 0.14	0.74 ± 0.14
Mdr1a/b$^{-/-}$*Bcrp1*$^{-/-}$	1.13 ± 0.13	1.13 ± 0.13	1.07 ± 0.03	1.08 ± 0.03

NOTE: Mean ± SD from 3 to 6 mice.

Published OnlineFirst June 30, 2009; DOI: 10.1158/0008-5472.CAN-09-0700

Results

Topotecan lactone plasma protein binding. The mean ± SD unbound fraction of plasma topotecan lactone was 30.1 ± 1.0% in wild-type, 29.2 ± 2.7% in *Mdr1a/b*$^{-/-}$, 30.9 ± 2.2% in *Bcrp1*$^{-/-}$, and 27.5 ± 1.9% in *Mdr1a/b*$^{-/-}$*Bcrp1*$^{-/-}$ mice. One-way ANOVA showed no significant difference among these results (P = 0.10).

Bcrp1 and P-gp enhance topotecan lactone penetration into the vCSF and decrease penetration into the brain ECF. For these studies, a microdialysis probe was placed in the lateral ventricle or the brain parenchymal tissue of each mouse, and proper placement was verified by postmortem histologic examination (Supplementary Fig. S1). After a single 4 mg/kg topotecan intravenous bolus injection, the mean ± SD vCSF-to-plasma ratio of unbound topotecan lactone ($AUC_{u,vCSF}$/ $AUC_{u,plasma}$) was 3.07 ± 0.09 in wild-type, 2.57 ± 0.17 in *Mdr1a/b*$^{-/-}$, 1.63 ± 0.12 in *Bcrp1*$^{-/-}$, and 0.86 ± 0.05 in *Mdr1a/b*$^{-/-}$*Bcrp1*$^{-/-}$ mice (Fig. 1). The mean ± SD *in vivo* probe recovery in these groups was 8.1 ± 2.4%, 7.1 ± 1.1%, 7.5 ± 1.5%, and 6.0 ± 0.6%, respectively. The CL_{in}-to-CL_{out} ratio at the BCB was consistent with the AUC ratio (Table 1).

The mean ± SD ECF-to-plasma AUC ratios ($AUC_{u,ECF}$/ $AUC_{u,plasma}$) of unbound topotecan lactone were 0.36 ± 0.06 in wild-type, 0.42 ± 0.06 in *Bcrp1*$^{-/-}$, and 0.89 ± 0.07 in *Mdr1a/b*$^{-/-}$/ *Bcrp1*$^{-/-}$ mice (Fig. 2). The topotecan lactone ECF concentrations in *Mdr1a/b*$^{-/-}$ mice were below the lower limit of detection of the assay. The *in vivo* probe recovery (mean ± SD) in these groups was 8.5 ± 2.4%, 5.4 ± 0.6%, and 4.3 ± 0.2%, respectively. The CL_{in}-to-CL_{out} ratio at the BBB was consistent with the AUC ratio (Table 1).

Effect of gefitinib on topotecan penetration of vCSF and ECF. After gefitinib pretreatment, no significant difference in topotecan lactone vCSF penetration (mean ± SD $AUC_{u,vCSF}/AUC_{u,plasma}$) was noted between wild-type and *Mdr1a/b*$^{-/-}$*Bcrp1*$^{-/-}$ mice (Fig. 3; 1.29 ± 0.09 versus 1.13 ± 0.13; P = 0.147, Student's t test), suggesting that gefitinib fully inhibited Bcrp1 and P-gp function at the BCB. For the BBB, mean ± SD $AUC_{u,ECF}/AUC_{u,plasma}$ ratios differed significantly between wild-type and *Mdr1a/b*$^{-/-}$*Bcrp1*$^{-/-}$ mice (Fig. 3; 0.74 ± 0.14 versus 1.07 ± 0.03; P < 0.05, Student's t test).

Preferential transport of topotecan lactone into the vCSF. We investigated whether unbound topotecan lactone would be preferentially transported *in vivo*. The mean ± SD vCSF lactone-to-carboxylate AUC ratio ($AUC_{lactone,vCSF}/AUC_{carboxylate,vCSF}$) was 5.7 ± 0.8 in wild-type, 3.9 ± 0.6 in *Mdr1a/b*$^{-/-}$, 3.6 ± 0.5 in *Bcrp1*$^{-/-}$, and 0.8 ± 0.2 in *Mdr1a/b*$^{-/-}$*Bcrp1*$^{-/-}$ mice. The ratios of the knockout groups were significantly different compared with the wild-type group (P = 0.003 for *Mdr1a/b*$^{-/-}$ and *Bcrp1*$^{-/-}$ mice and P < 0.001 for *Mdr1a/b*$^{-/-}$*Bcrp1*$^{-/-}$ mice, ANOVA with post hoc t test with Bonferroni correction). The mean ± SD plasma lactone-to-carboxylate AUC ratio ($AUC_{lactone,plasma}$/ $AUC_{carboxylate,plasma}$) was not significantly different between wild-type and *Mdr1a/b*$^{-/-}$*Bcrp1*$^{-/-}$ mice (1.24 ± 0.38 versus 0.95 ± 0.28; P = 0.11, Student's t test). Different $AUC_{lactone}$/ $AUC_{carboxylate}$ ratios in vCSF but similar ones in plasma suggest the preferential active transport of topotecan lactone across the BCB by these ABC transporters.

Saos2-BCRP cells transport topotecan lactone. To determine whether BCRP is capable of specifically transporting topotecan lactone, we evaluated topotecan lactone efflux in cells overexpressing BCRP. After a 1-min incubation with topotecan lactone (stable at pH 6), the mean ± SD intracellular topotecan lactone concentration was significantly higher in Saos2-pcDNA cells than in Saos2-BCRP cells (0.063 ± 0.01 versus 0.043 ± 0.005 ng/μg protein; P = 0.05, Student's t test). A similar difference was observed after a 30-min incubation at the same pH (0.039 ± 0.003 ng/μg in Saos2-pcDNA versus 0.026 ± 0.004 ng/μg in Saos2-BCRP cells; P = 0.05). Topotecan carboxylate was not detected at pH 6. We observed no difference in intracellular topotecan carboxylate accumulation between Saos2-pcDNA and Saos2-BCRP cells at pH 8 (data not shown).

***Mdr1a/b*$^{-/-}$ mice overexpress Bcrp1 protein at the BBB.** Because topotecan lactone ECF concentrations in the *Mdr1a/b*$^{-/-}$

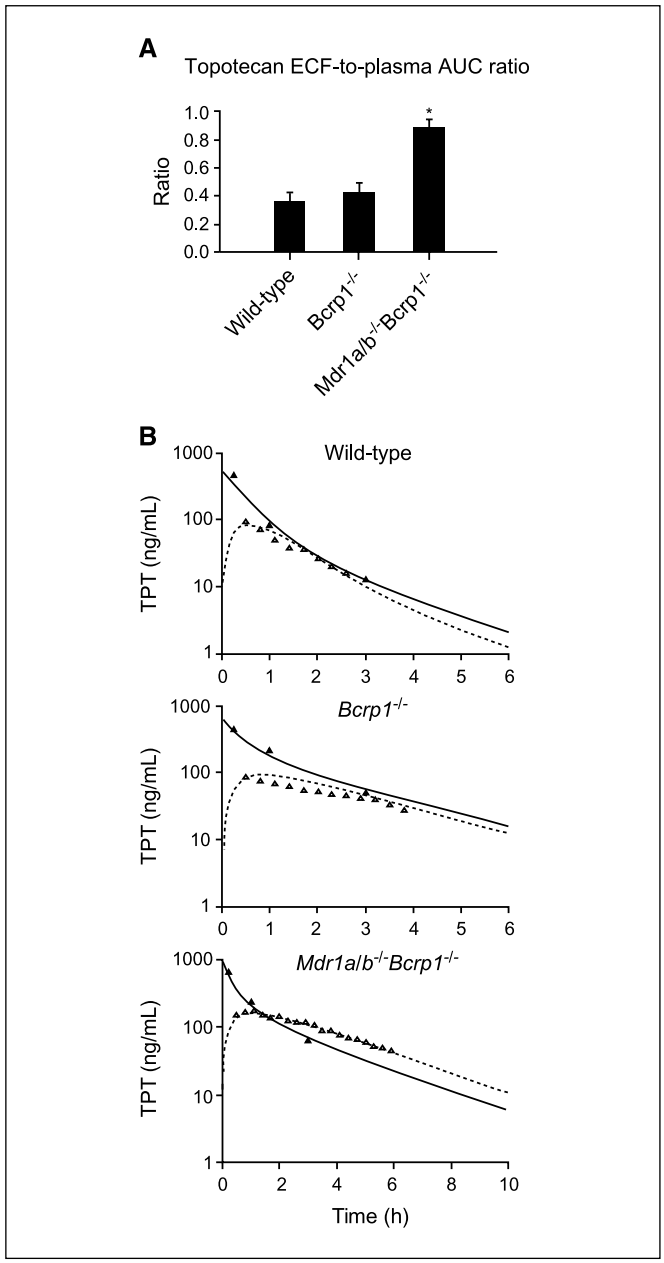

Figure 2. Topotecan lactone penetration into brain ECF after a bolus intravenous dose of 4 mg/kg topotecan. *A,* brain ECF-to-plasma AUC ratio of unbound topotecan lactone (mean ± SD from 3 to 5 mice). P < 0.001, one-way ANOVA; *, P < 0.001, post hoc t test with Bonferroni correction, of each knockout model compared with wild-type mice. *B,* representative unbound topotecan lactone concentration-time plots in ECF (△) and plasma (▲) in wild-type, *Bcrp1*$^{-/-}$, and *Mdr1a/b*$^{-/-}$*Bcrp1*$^{-/-}$ mice. Model-fitted curves are represented for plasma and brain pharmacokinetic data.

Published OnlineFirst June 30, 2009; DOI: 10.1158/0008-5472.CAN-09-0700

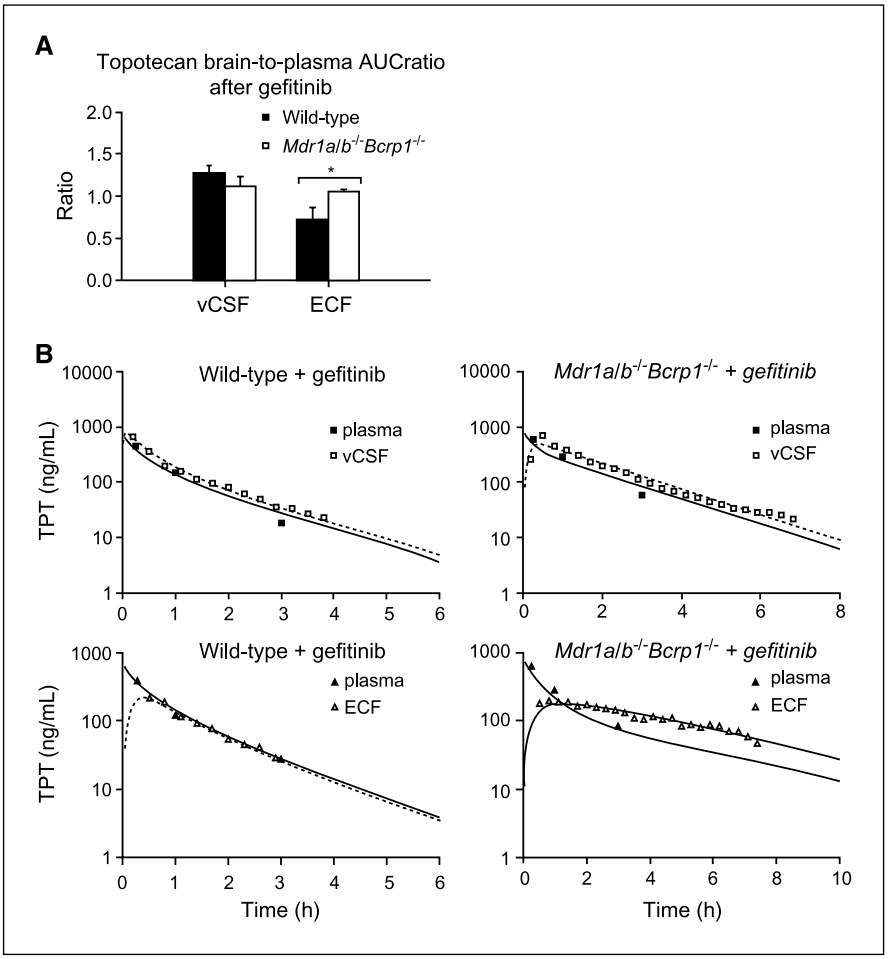

Figure 3. Topotecan penetration into vCSF and brain ECF after 200 mg/kg gefitinib by oral gavage followed by a bolus intravenous dose of 4 mg/kg topotecan. *A,* brain vCSF-to-plasma and ECF-to-plasma AUC ratios of unbound topotecan lactone in wild-type and *Mdr1a/b*$^{-/-}$*Bcrp1*$^{-/-}$ mice (mean ± SD from 3 mice). *, $P < 0.05$, Student's *t* test. *B,* representative concentration-time plots of unbound topotecan lactone in vCSF (□), ECF (△), and plasma (■,▲) of wild-type and *Mdr1a/b*$^{-/-}$*Bcrp1*$^{-/-}$ mice. Model-fitted curves are represented for plasma and brain pharmacokinetic data.

mice were below the lower limit of detection, we hypothesized that Bcrp1 protein might be overexpressed in these animals, thereby increasing the overall drug efflux into the brain microvessels. A semiquantitative immunohistochemical analysis of Bcrp1 expression in the microvascular endothelium in wild-type and *Mdr1a/b*$^{-/-}$ mice showed greater expression in the *Mdr1a/b*$^{-/-}$ mice, with no apparent differences in vessel density (Fig. 4).

Discussion

The active transport mechanisms that control topotecan penetration and pharmacokinetics in different CNS compartments have not been well described previously. By using our modified surgical procedure (25), microdialysis sampling, transporter-deficient mice, and pharmacokinetic modeling, we elucidated the roles of Bcrp1 and P-gp in the differential penetration of the CNS barriers by topotecan. Although these transporters enhanced the entry of topotecan into the CSF through the BCB, they restricted exposure of parenchymal brain to topotecan by acting as efflux transporters at the BBB. Our results may be clinically relevant in several ways. First, they may explain why topotecan is more active against CNS tumors that spread via leptomeningeal route than those located in the brain hemispheres. Second, they indicate that the use of CSF drug levels to predict CNS penetration warrants reconsideration. Finally, our results may help to predict the effects of ABC transporter inhibitors on the efficacy of chemotherapy for CNS tumors.

Our results suggest that Bcrp1 plays a major role, whereas P-gp plays a lesser role in transporting topotecan into the vCSF. Both proteins are present in the ependymal cells of the choroid plexus (17, 33, 34), and the role of P-gp in the active efflux of potentially toxic substances into the CSF has been described (33, 35). However, ours is the first study to show that Bcrp1 plays a significant role in this BCB-mediated protective mechanism. There appeared to be no functional redundancy between Bcrp1 and P-gp at the BCB in our mouse models, as animals deficient in either protein showed a correspondingly reduced topotecan vCSF penetration. Interestingly, the vCSF-to-plasma AUC ratio in *Mdr1a/b*$^{-/-}$*Bcrp1*$^{-/-}$ mice was <1.0, which suggests active efflux from the vCSF compartment (31). This result may be explained by our previous finding that Mrp4 mediates efflux of topotecan from vCSF, a mechanism that opposes Bcrp1 and P-gp activity at the BCB (18).

In studies of the BBB penetration of topotecan, the loss of either transporter appeared to be compensated or even surpassed by overexpression of the other (Fig. 2). The nondeleted transporter may have been up-regulated at the BBB in these mice. In the *Mdr1a*$^{-/-}$ model, for example, Bcrp1 mRNA is reportedly up-regulated 3-fold in the cerebral microvessels (36), which is consistent with the stronger Bcrp1 staining we observed in *Mdr1a/b*$^{-/-}$ mice compared with wild-type mice (Fig. 4). Although

Published OnlineFirst June 30, 2009; DOI: 10.1158/0008-5472.CAN-09-0700

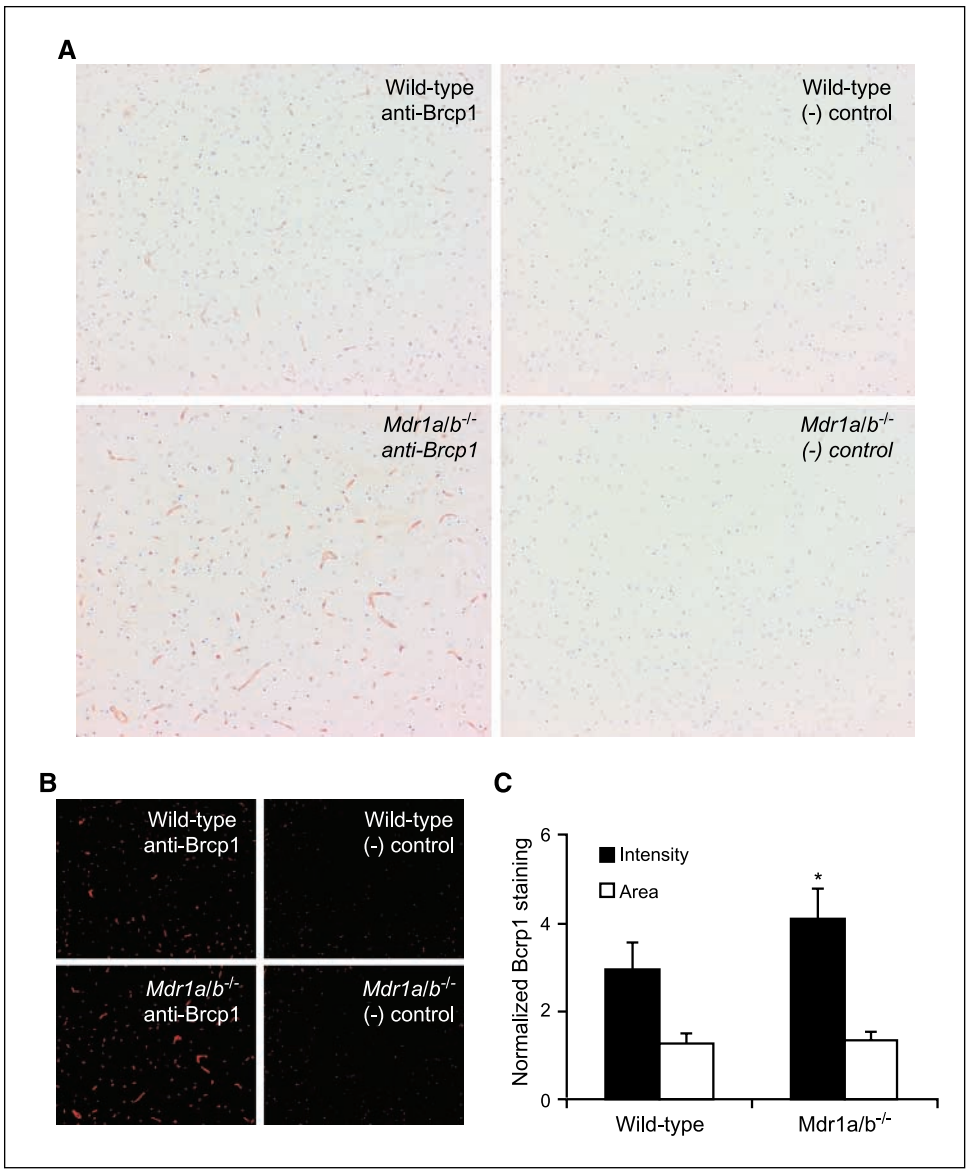

Figure 4. Immunohistochemical staining of Bcrp1 in wild-type and *Mdr1a/b*$^{-/-}$ mice. *A,* Bcrp1 staining is observed in the brain capillaries of wild-type and *Mdr1a/b*$^{-/-}$ mice, with stronger staining in the *Mdr1a/b*$^{-/-}$ strain. Negative controls for wild-type and *Mdr1a/b*$^{-/-}$ mice are also shown. *B,* processed images from *A*, showing the stained areas in red. *C,* quantification of the intensity and area of Bcrp1 staining. Mean ± SD of six different fields from two different sections normalized to the mean values quantified in negative control slides. *, $P = 0.012$, Student's *t* test.

Bcrp1 protein in whole-brain tissue homogenates was recently reported not to be overexpressed in the *Mdr1a/b*$^{-/-}$ murine model compared with wild-type mice (19), the change in protein expression in the microvasculature is likely to have been masked in that study's Western blots of whole-brain homogenates. In the *Bcrp1*$^{-/-}$ model, the ECF-to-plasma AUC ratio was comparable with that in the wild-type mice. To our knowledge, these are the first findings to suggest compensatory mechanisms for the loss of Bcrp1 function. Our results agree with those of previous studies using the *Bcrp1*$^{-/-}$ mouse model, which found no increased BBB penetration *in vivo* by drugs that are Bcrp1 substrates *in vitro* (19, 37). Compensatory up-regulation of the nondeleted transporter would mean that neither the *Mdr1a/b*$^{-/-}$ nor the *Bcrp1*$^{-/-}$ model can reliably be used to distinguish the roles of P-gp or Bcrp1 in BBB transport *in vivo*. Therefore, results obtained using animal models with single-transporter deletions should be interpreted cautiously. However, the significantly higher ECF-to-plasma AUC ratio of unbound topotecan lactone in the *Mdr1a/b*$^{-/-}$*Bcrp1*$^{-/-}$ mice compared with wild-type mice in our study (Table 1) reveals that P-gp and Bcrp1 work together in restricting topotecan penetration through the BBB.

The markedly different ECF and vCSF topotecan penetration we observed highlights the limitations of using CSF sampling or whole-brain homogenates to study CNS drug penetration. Studies using total homogenates may misinterpret drug penetration of brain parenchyma, as they include both protein-bound and unbound drug fractions from brain vessels, brain ECF, brain CSF, and brain intracellular fluid. A recently published study used the total (lactone + carboxylate) topotecan concentration values in whole-brain homogenates from knockout animals to define the roles of P-gp and Bcrp1 in brain penetration, concluding that both transporters act together at the BBB and inhibit topotecan penetration of the brain (19). However, this method was unable to define intercompartmental drug kinetics. Several studies have shown differential drug distribution in CSF compared with brain ECF. For example, Venkatakrishnan and colleagues found that CP-615,003, a $GABA_A$ receptor agonist confirmed to be a P-gp substrate, accumulates in rat CSF 7-fold higher than in ECF (38).

Published OnlineFirst June 30, 2009; DOI: 10.1158/0008-5472.CAN-09-0700

Similar reports about other drugs are available (39, 40). It was recently postulated that the CSF-to-plasma ratio of free drug can be used to estimate the brain parenchymal penetration of highly permeant drugs that are not efflux transporter substrates (41).

Interestingly, we observed preferential active transport *in vivo* of the active topotecan lactone over the inactive carboxylate. Transport of topotecan lactone by human BCRP was also confirmed *in vitro*. In contrast, topotecan carboxylate transport by BCRP was not detected, although at pH 8 (required to stabilize the carboxylate in our *in vitro* experiment), the activity of BCRP could be altered (42). These findings highlight the relevance of pharmacologic strategies that target topotecan transporters to modulate the concentration of active drug in the treated tissues. The tyrosine kinase inhibitor gefitinib provides an example. In our previous studies, gefitinib increased oral absorption and decreased systemic clearance of topotecan and irinotecan (23, 43). In the present study, we hypothesized that if gefitinib fully inhibits Bcrp1 and P-gp function at the BBB or BCB, similar topotecan AUC ratios would be observed in wild-type and *Mdr1a/b*$^{-/-}$*Bcrp1*$^{-/-}$ mice treated with gefitinib. The wild-type and *Mdr1a/b*$^{-/-}$*Bcrp1*$^{-/-}$ mice did have similar AUC ratios in the BCB penetration study, but in the BBB comparisons the brain-to-plasma ratio was significantly greater in *Mdr1a/b*$^{-/-}$*Bcrp1*$^{-/-}$ mice. Assuming that other unknown transport mechanisms at the BBB are equal in both mouse models, this finding suggests that gefitinib can fully inhibit Bcrp1 and P-gp at the BCB but not at the BBB (see Supplementary Text for analysis). Alternatively, transport mechanisms other than P-gp and Bcrp1 may act differently either at the BCB, the BBB, or both barriers of the wild-type and *Mdr1a/b*$^{-/-}$*Bcrp1*$^{-/-}$ mice. Such putative transport mechanisms appear to be active at the BCB of the *Mdr1a/b*$^{-/-}$*Bcrp1*$^{-/-}$ mice, because a significant increase in topotecan vCSF penetration was noted when these animals received gefitinib (see representative plots for *Mdr1a/b*$^{-/-}$*Bcrp1*$^{-/-}$ mice in Figs. 1 and 3). This finding may reflect either gefitinib inhibition of ABC transporters, the action of which opposes that of P-gp and Bcrp1 at the BCB (e.g., Mrp4; ref. 18), or the widespread presence of the organic anion transporter and organic anion-transporting peptides at the BBB and BCB in rodents (20, 44, 45). OAT3 is present in the renal basolateral membrane, where it enhances renal tubular secretion of topotecan carboxylate in the rat (46). *In vitro* studies have found that human OAT3 transports topotecan carboxylate (46). Because it is localized on the apical border of the choroid plexus at the BCB and on endothelial cells at the BBB in rats and mice (47), OAT3 could oppose the transport functions of Bcrp1 and P-gp but cooperate with that of Mrp4 to restrict topotecan penetration into CSF. Similarly, human OATP1B1 can mediate uptake of SN-38 (the active metabolite of irinotecan) in the liver (48). Although human OATP1B1 is not known to be expressed in the CNS, rat OATP2 (its counterpart) is found on both apical and basolateral sides of brain capillary endothelial cells and on the basolateral side of choroid plexus epithelial cells. Therefore, it may enhance topotecan penetration of the CSF, as do Bcrp1 and P-gp (49).

To summarize, topotecan influx into the vCSF and efflux from the brain parenchyma via the ECF are driven by the transporters P-gp and Bcrp1 in a manner consistent with their cellular orientation at the BCB and BBB. The blockade of P-gp and Bcrp1 activity by treatment with tyrosine kinase inhibitors reverses these effects, causing topotecan depletion in the vCSF and accumulation in the ECF. Although this study focused on a specific drug, we will use the same methods and models for investigations aimed at improving other chemotherapies for CNS tumors located in specific CNS compartments. Increasing evidence shows that histologically identical brain tumors can differ molecularly according to the site of origin of their precursors in the brain and thus may differ in their susceptibility to molecularly targeted chemotherapy agents (50). We propose that the site-specific penetration of candidate agents should be considered when selecting optimal chemotherapy treatments.

Disclosure of Potential Conflicts of Interest

No potential conflicts of interest were disclosed.

Acknowledgments

Received 2/23/09; revised 4/23/09; accepted 5/13/09; published OnlineFirst 6/30/09.

Grant support: USPHS grants CA23099, CA21765, and GM071321-04 and American Lebanese Syrian Associated Charities.

The costs of publication of this article were defrayed in part by the payment of page charges. This article must therefore be hereby marked *advertisement* in accordance with 18 U.S.C. Section 1734 solely to indicate this fact.

We thank Sharon Naron for editorial assistance.

References

1. Gottardo NG, Gajjar A. Chemotherapy for malignant brain tumors of childhood. J Child Neurol 2008;23:1149–59.
2. Rutkowski S, Bode U, Deinlein F, et al. Treatment of early childhood medulloblastoma by postoperative chemotherapy alone. N Engl J Med 2005;352:978–86.
3. Broniscer A, Chintagumpala M, Fouladi M, et al. Temozolomide after radiotherapy for newly diagnosed high-grade glioma and unfavorable low-grade glioma in children. J Neurooncol 2006;76:313–9.
4. Houghton PJ, Cheshire PJ, Hallman JD, et al. Efficacy of topoisomerase I inhibitors, topotecan and irinotecan, administered at low dose levels in protracted schedules to mice bearing xenografts of human tumors. Cancer Chemother Pharmacol 1995;36:393–403.
5. Hare CB, Elion GB, Houghton PJ, et al. Therapeutic efficacy of the topoisomerase I inhibitor 7-ethyl-10-(4-[1-piperidino]-1-piperidino)-carbonyloxy-camptothecin against pediatric and adult central nervous system tumor xenografts. Cancer Chemother Pharmacol 1997; 39:187–91.
6. Pawlik CA, Houghton PJ, Stewart CF, Cheshire PJ, Richmond LB, Danks MK. Effective schedules of exposure of medulloblastoma and rhabdomyosarcoma xenografts to topotecan correlate with *in vitro* assays. Clin Cancer Res 1998;4:1995–2002.
7. Zamboni WC, Stewart CF, Thompson J, et al. Relationship between topotecan systemic exposure and tumor response in human neuroblastoma xenografts. J Natl Cancer Inst 1998;90:505–11.
8. Stewart CF, Iacono LC, Chintagumpala M, et al. Results of a phase II upfront window of pharmacokinetically guided topotecan in high-risk medulloblastoma and supratentorial primitive neuroectodermal tumor. J Clin Oncol 2004;22:3357–65.
9. Bernier-Chastagner V, Grill J, Doz F, et al. Topotecan as a radiosensitizer in the treatment of children with malignant diffuse brainstem gliomas: results of a French Society of Paediatric Oncology phase II study. Cancer 2005;104:2792–7.
10. Chintagumpala MM, Friedman HS, Stewart CF, et al. A phase II window trial of procarbazine and topotecan in children with high-grade glioma: a report from the Children's Oncology Group. J Neurooncol 2006;77:193–8.
11. de Lange EC. Potential role of ABC transporters as a detoxification system at the blood-CSF barrier. Adv Drug Deliv Rev 2004;56:1793–809.
12. Zheng W, Chodobski A. The blood-cerebrospinal fluid barrier. Boca Raton (FL): CRC Press; 2005.
13. Nag S. The blood-brain barrier. Biology and research protocols. Totowa (NJ): Humana Press; 2003.
14. Motl S, Zhuang Y, Waters CM, Stewart CF. Pharmacokinetic considerations in the treatment of CNS tumours. Clin Pharmacokinet 2006;45:871–903.
15. Hendricks CB, Rowinsky EK, Grochow LB, Donehower RC, Kaufmann SH. Effect of P-glycoprotein expression on the accumulation and cytotoxicity of topotecan (SK&F 104864), a new camptothecin analogue. Cancer Res 1992;52:2268–78.
16. Maliepaard M, van Gastelen MA, Tohgo A, et al. Circumvention of breast cancer resistance protein (BCRP)-mediated resistance to camptothecins *in vitro* using non-substrate drugs or the BCRP inhibitor GF120918. Clin Cancer Res 2001;7:935–41.

17. Zhuang Y, Fraga CH, Hubbard KE, et al. Topotecan central nervous system penetration is altered by a tyrosine kinase inhibitor. Cancer Res 2006;66:11305–13.

18. Leggas M, Adachi M, Scheffer GL, et al. Mrp4 confers resistance to topotecan and protects the brain from chemotherapy. Mol Cell Biol 2004;24:7612–21.

19. de Vries NA, Zhao J, Kroon E, Buckle T, Beijnen JH, van Tellingen O. P-glycoprotein and breast cancer resistance protein: two dominant transporters working together in limiting the brain penetration of topotecan. Clin Cancer Res 2007;13:6440–9.

20. Loscher W, Potschka H. Drug resistance in brain diseases and the role of drug efflux transporters. Nat Rev Neurosci 2005;6:591–602.

21. Maliepaard M, van Gastelen MA, de Jong LA, et al. Overexpression of the BCRP/MXR/ABCP gene in a topotecan-selected ovarian tumor cell line. Cancer Res 1999;59:4559–63.

22. Tian Q, Zhang J, Tan TM, et al. Human multidrug resistance associated protein 4 confers resistance to camptothecins. Pharm Res 2005;22:1837–53.

23. Leggas M, Panetta JC, Zhuang Y, et al. Gefitinib modulates the function of multiple ATP-binding cassette transporters *in vivo*. Cancer Res 2006;66:4802–7.

24. Li H, Jin HE, Kim W, et al. Involvement of P-glycoprotein, multidrug resistance protein 2 and breast cancer resistance protein in the transport of belotecan and topotecan in Caco-2 and MDCKII Cells. Pharm Res 2008;25:2601–12.

25. Shen J, Fraga C, Calabrese C, McCarville MB, Schaiquevich P, Stewart CF. A modified surgical procedure for microdialysis probe implantation in the lateral ventricle of a FVB mouse. J Pharm Sci 2008;97:5013–23.

26. Leggas M, Zhuang Y, Welden J, Self Z, Waters CM, Stewart CF. Microbore HPLC method with online microdialysis for measurement of topotecan lactone and carboxylate in murine CSF. J Pharm Sci 2004;93:2284–95.

27. Kehr J, Yoshitake T, Wang FH, et al. Microdialysis in freely moving mice: determination of acetylcholine, serotonin and noradrenaline release in galanin transgenic mice. J Neurosci Methods 2001;109:71–80.

28. Hing JP, Woolfrey SG, Greenslade D, Wright PM. Analysis of toxicokinetic data using NONMEM: impact of quantification limit and replacement strategies for censored data. J Pharmacokinet Pharmacodyn 2001;28:465–79.

29. Beal SL. NONMEM users' guide. Introduction to version IV. Ellicott City (MD): ICON Development Solutions; 2006.

30. D'Argenio DZ, Schumitzky A. ADAPT II user's guide: pharmacokinetic/pharmacodynamic systems analysis software. Los Angeles: Biomedical Simulations Resource; 1997.

31. Hammarlund-Udenaes M, Friden M, Syvanen S, Gupta A. On the rate and extent of drug delivery to the brain. Pharm Res 2008;25:1737–50.

32. Wong SL, Van Belle K, Sawchuk RJ. Distributional transport kinetics of zidovudine between plasma and brain extracellular fluid/cerebrospinal fluid in the rabbit: investigation of the inhibitory effect of probenecid utilizing microdialysis. J Pharmacol Exp Ther 1993;264:899–909.

33. Rao VV, Dahlheimer JL, Bardgett ME, et al. Choroid plexus epithelial expression of MDR1 P glycoprotein and multidrug resistance-associated protein contribute to the blood-cerebrospinal-fluid drug-permeability barrier. Proc Natl Acad Sci U S A 1999;96:3900–5.

34. Warren KE, Patel MC, McCully CM, Montuenga LM, Balis FM. Effect of P-glycoprotein modulation with cyclosporin A on cerebrospinal fluid penetration of doxorubicin in non-human primates. Cancer Chemother Pharmacol 2000;45:207–12.

35. Chen J, Balmaceda C, Bruce JN, et al. Tamoxifen paradoxically decreases paclitaxel deposition into cerebrospinal fluid of brain tumor patients. J Neurooncol 2006;76:85–92.

36. Cisternino S, Mercier C, Bourasset F, Roux F, Scherrmann JM. Expression, up-regulation, and transport activity of the multidrug-resistance protein Abcg2 at the mouse blood-brain barrier. Cancer Res 2004;64:3296–301.

37. Giri N, Shaik N, Pan G, et al. Investigation of the role of breast cancer resistance protein (Bcrp/Abcg2) on pharmacokinetics and central nervous system penetration of abacavir and zidovudine in the mouse. Drug Metab Dispos 2008;36:1476–84.

38. Venkatakrishnan K, Tseng E, Nelson FR, et al. Central nervous system pharmacokinetics of the Mdr1 P-glycoprotein substrate CP-615,003: intersite differences and implications for human receptor occupancy projections from cerebrospinal fluid exposures. Drug Metab Dispos 2007;35:1341–9.

39. Stain-Texier F, Boschi G, Sandouk P, Scherrmann JM. Elevated concentrations of morphine 6-β-D-glucuronide in brain extracellular fluid despite low blood-brain barrier permeability. Br J Pharmacol 1999;128:917–24.

40. Kaddoumi A, Choi SU, Kinman L, et al. Inhibition of P-glycoprotein activity at the primate blood-brain barrier increases the distribution of nelfinavir into the brain but not into the cerebrospinal fluid. Drug Metab Dispos 2007;35:1459–62.

41. Liu X, Chen C, Smith BJ. Progress in brain penetration evaluation in drug discovery and development. J Pharmacol Exp Ther 2008;325:349–56.

42. Breedveld P, Pluim D, Cipriani G, et al. The effect of low pH on breast cancer resistance protein (ABCG2)-mediated transport of methotrexate, 7-hydroxymethotrexate, methotrexate diglutamate, folic acid, mitoxantrone, topotecan, and resveratrol in *in vitro* drug transport models. Mol Pharmacol 2007;71:240–9.

43. Stewart CF, Leggas M, Schuetz JD, et al. Gefitinib enhances the antitumor activity and oral bioavailability of irinotecan in mice. Cancer Res 2004;64:7491–9.

44. Zair ZM, Eloranta JJ, Stieger B, Kullak-Ublick GA. Pharmacogenetics of OATP (SLC21/SLCO), OAT and OCT (SLC22) and PEPT (SLC15) transporters in the intestine, liver and kidney. Pharmacogenomics 2008;9:597–624.

45. Ito K, Suzuki H, Horie T, Sugiyama Y. Apical/basolateral surface expression of drug transporters and its role in vectorial drug transport. Pharm Res 2005;22:1559–77.

46. Matsumoto S, Yoshida K, Ishiguro N, Maeda T, Tamai I. Involvement of rat and human organic anion transporter 3 in the renal tubular secretion of topotecan [(*S*)-9-dimethylaminomethyl-10-hydroxy-camptothecin hydrochloride]. J Pharmacol Exp Ther 2007;322:1246–52.

47. Nagata Y, Kusuhara H, Endou H, Sugiyama Y. Expression and functional characterization of rat organic anion transporter 3 (rOat3) in the choroid plexus. Mol Pharmacol 2002;61:982–8.

48. Nozawa T, Minami H, Sugiura S, Tsuji A, Tamai I. Role of organic anion transporter OATP1B1 (OATP-C) in hepatic uptake of irinotecan and its active metabolite, 7-ethyl-10-hydroxycamptothecin: *in vitro* evidence and effect of single nucleotide polymorphisms. Drug Metab Dispos 2005;33:434–9.

49. Gao B, Stieger B, Noe B, Fritschy JM, Meier PJ. Localization of the organic anion transporting polypeptide 2 (Oatp2) in capillary endothelium and choroid plexus epithelium of rat brain. J Histochem Cytochem 1999;47:1255–64.

50. Gilbertson RJ, Ellison DW. The origins of medulloblastoma subtypes. Annu Rev Pathol 2008;3:341–65.

Cancer Research
The Journal of Cancer Research (1916–1930) | The American Journal of Cancer (1931–1940)

AACR American Association for Cancer Research

Compartment-Specific Roles of ATP-Binding Cassette Transporters Define Differential Topotecan Distribution in Brain Parenchyma and Cerebrospinal Fluid

Jun Shen, Angel M. Carcaboso, K. Elaine Hubbard, et al.

Cancer Res Published OnlineFirst June 30, 2009.